Physica Scripta

INCLUSIVE PUBLISHING
TRUSTED SCIENCE

PAPER

Photocatalytic activity of hybrid Ag/Er:ZnO nanoparticles synthesized by pulsed laser ablation in distilled water

To cite this article: Samah M Ahmed and Hisham Imam 2023 *Phys. Scr.* **98** 095934

View the article online for updates and enhancements.

You may also like

- Luminescent and lasing characteristics of polycrystalline Cr:Fe:ZnSe exited at 2.09 and 2.94 μm wavelengths
V A Antonov, K N Firsov, E M Gavrishchuk et al.
- High-efficiency broadly tunable Cr:ZnSe single crystal laser pumped by Tm:YLF laser
Y F Dai, Y Y Li, X Zou et al.
- Photoluminescence of rare-earth ion (Eu^{3+}, Tm^{3+}, and Er^{3+})-doped and co-doped $ZnNb_2O_6$ for solar cells
Sen-Pei Gao, , Yan-Nan Qian et al.

This content was downloaded from IP address 193.227.11.119 on 20/11/2023 at 16:00

Physica Scripta

PAPER

Photocatalytic activity of hybrid Ag/Er:ZnO nanoparticles synthesized by pulsed laser ablation in distilled water

RECEIVED
16 May 2023

REVISED
10 July 2023

ACCEPTED FOR PUBLICATION
25 July 2023

PUBLISHED
17 August 2023

Samah M Ahmed[1,2,*] **and Hisham Imam**[1]

[1] National Institute of Laser Enhanced Sciences, Cairo University, PO Box 11316, Cairo, Egypt
[2] Physics Department, Faculty of Science & Arts, Al Jouf University, Tabarjal, Saudi Arabia
[*] Author to whom any correspondence should be addressed.

E-mail: samahmha@niles.edu.e.g

Keywords: ZnO nanoparticles, erbium oxide dopant, silver nanoparticles, pulsed laser ablation in water, photocatalysis

Supplementary material for this article is available online

Abstract

We have studied the photocatalytic performance of ZnO, Er:ZnO, hybrid Ag/ZnO, and Ag/Er:ZnO colloidal nanoparticles (NPs) synthesized by pulsed laser ablation of stoichiometric targets and silver plate in double distilled water. The x-ray diffraction (XRD) analysis revealed the polycrystalline structure of the ablated NPs. The morphology of the nanoparticles was examined by the transmission electron microscope (TEM). The optical properties of the prepared colloidal NPs were investigated by the UV-visible absorption and photoluminescence spectroscopies. The photodegradation of the Rhodamine 6G organic dye was utilized to evaluate the photocatalytic activity of the produced colloidal NPs under illumination by UV light. The hybrid Ag/Er:ZnO colloidal NPs showed enhanced photodegradation efficiency of 96.4%, after 45 min of UV irradiation, compared to 79.7% of the pristine ZnO NPs. The obtained results point out the enhancing effect of the dopants on the photocatalytic performance of ZnO, and further demonstrate the pulsed laser ablation of bulk materials in pure water as a fast and eco-friendly technique for producing efficient nanoparticle photocatalysts.

1. Introduction

The removal of hazardous organic pollutants from the industrial wastewater by photocatalysis is among the known strategies used for wastewater treatment. In the last decades, developing zinc oxide (ZnO) nanomaterials for photocatalytic applications has attracted a growing interest due to the distinctive properties of ZnO semiconductor, beside its non-toxicity, good stability, and availability [1–7].

Moreover, many reported studies have shown that ZnO modified with appropriate dopants (such as rare-Earth (RE) elements and noble metals) can exhibit improved properties compared to the pristine ZnO in different applications [8–15]. For example, the photocatalytic properties of ZnO nanoparticles have been enhanced upon doping with europium ions (Eu^{3+}) [16–18], erbium ions (Er^{3+}) [19–25], and by hybridization with selected noble metal such as silver (Ag) [26–39]. The observed effective separation of the photo-generated charges in ZnO has been attributed to the electron-scavenger effect of the noble metal [26] and the point defects introduced by RE-doping [23]. In addition, the upconverted optical emission of Er^{3+} ions dopant has been reported to increase the charge carrier density and hence the photocatalytic efficiency of ZnO [19, 20].

The preparation technique can also affect the properties of ZnO nanomaterials [40, 41]. Pulsed laser ablation in liquid media (PLAL) is a rapid, straight forward, and eco-friendly technique by which nanoparticles with high purity can be synthesized without reducing or capping agents and at the ambient conditions [42–48]. In the literature there are many studies reported the synthesis of ZnO NPs by pulsed laser ablation of Zn metal or ZnO target in liquid media. For instance, Guillen *et al* reported on the preparation of ZnO NPs by pulsed laser ablation of Zn metal in distilled water at different temperatures [49]. Camarda *et al* have prepared crystalline and luminescent ZnO NPs by ultra-short femtosecond pulsed laser ablation of Zn plate in deionized water [50].

© 2023 IOP Publishing Ltd

Chen *et al* have synthesized ZnO NPs by pulsed laser ablation of Zn powder suspending in deionized water [51]. Khudiar *et al* have prepared ZnO NPs via pulsed laser ablation of Zn target in methanol, for sensing NO_2 gas [52]. Also, ZnO NPs with antibacterial activity [53], and Zn@ZnO core–shell nanostructures for sensing hydroquinone [54] have been synthesized by PLAL. In addition, Ag/ZnO nanoparticles with enhanced photocatalytic activity [36, 55] and anticancer nature [56], have been produced by PLAL using Zn and Ag metallic targets [55, 56] and Ag-coated ZnO target [36] in water. Furthermore, Ag/Au-ZnO plasmonic hybrid nanomaterials have been synthesized by pulsed laser ablation of Ag/Au bimetallic in water followed by mixing with ZnO nano-powder and by laser irradiation of the mixture [57].

To the best of our knowledge, there are few reported studies on the synthesis of RE-doped ZnO colloidal NPs by PLAL. Tarasenka *et al* have demonstrated Nd^{3+}-doped ZnO nanocrystals, prepared by pulsed laser ablation of Zn metal in an aqueous solution of neodymium nitrate, for NIR-II fluorescence bioimaging [58]. Katsuki *et al* have synthesized luminescent Eu^{3+}:ZnO NPs by PLAL using Eu-doped ZnO sintered disk in SDS surfactant solution [59]. In our previous study [16], we reported on the photocatalytic activity of Au/Eu:ZnO NPs prepared by pulsed laser ablation of Eu-doped ZnO sintered target and gold plate in distilled water. And herein, as an extension of our previous one, we report on the photocatalytic performance of hybrid Ag/Er:ZnO colloidal nanoparticles synthesized by pulsed laser ablation of Er:ZnO sintered pellet and silver metallic plate in distilled water. The motivation of the current work was to evaluate the reproducibility and reliability of the pulsed laser ablation in liquid (PLAL) technique to produce hybrid noble metal/rare-Earth doped semiconductor colloidal nanoparticles with enhanced photocatalytic performance. We replaced both the rare-Earth dopant and the noble metal nanoparticles: the trivalent Europium oxide Eu^{3+} is replaced by Erbium ions Er^{3+}, and the noble metal Au was replaced by Ag.

2. Materials and methods

In the present study, ZnO, Er:ZnO, Ag/ZnO and Ag/Er:ZnO colloidal nanoparticles have been synthesized by pulsed laser ablation of the stoichiometric bulk targets in double distilled water, as adopted from our previous reported study [16]. The undoped and Er-doped ZnO (with doping concentration of 1 mol % Er_2O_3) sintered ceramic targets have been produced by the conventional solid-state reaction, and the details of the sintering process are found in [60].

The PLAL experiment was conducted using a pulsed Nd^{3+}:YAG laser (Continuum SL-10) operating at the following laser parameters: laser beam wavelength of 1.064 μm, pulse duration of about 8 ns, pulse repetition rate of 10 Hz, and laser energy of $\sim$ 50 mJ/pulse. The focused laser beam was incident vertically on the target which was immersed in 15 ml of double distilled water. The apparent crater spot size of the focused laser beam was $\sim$ 0.2 mm and the corresponding energy density delivered to the target surface was estimated to be $\sim$ 160 J cm^{-2}. The ablation time was kept at 10 min, and the beaker was rotated slowly to keep homogeneous ablation of the target surface and reduce the deeply ablated traces. Finally, the hybrid Ag/ZnO and Ag/Er:ZnO colloidal NPs have been prepared by ablating a high purity silver plate (Fine Silver 999) immersed in the obtained ZnO and Er:ZnO NPs colloidals, respectively, with the same laser ablation parameters as above (laser energy and ablation time of $\sim$ 50 mJ/pulse and 10 min, respectively). Continuous magnetic stirring was provided during the laser ablation.

The crystallinity of the ablated nanoparticles was examined by an x-ray diffractometer (Bruker D8-Discover) equipped with a CuKα radiation source with wavelength of 1.5406°A. The as-prepared NPs colloidal solutions were dropped onto glass slides and dried at 100 °C for few minutes in a furnace, to form powder films suitable for the XRD measurements. Moreover, an energy-dispersive x-ray spectrometer (EDXS), equipped on a scanning electron microscope (TESCAN-VEGA3), was utilized to identify the constituent elements in the hybrid Ag/Er:ZnO sample. The size and shape of the laser-ablated nanoparticles were investigated by a high-resolution transmission electron microscope (HR-TEM) (model: JEM-2100). The UV-visible absorbance spectra of the colloidal NPs were obtained by a dual-beam spectrophotometer (Jasco V-750). The photoluminescence (PL) spectra of the prepared samples were recorded at room-temperature by a Hitachi Fluorescence Spectrophotometer (F-7100), at excitation wavelength of 325 nm (to induce band-to-band transitions of ZnO semiconductor).

The photocatalytic properties of the colloidal nanoparticles were examined by using Rhodamine 6G (R6G) dye as a model organic pollutant. The details of the photocatalytic experiment are found elsewhere [16]. Briefly, in each photocatalytic experiment, after well mixing the prepared colloidal NPs with the R6G aqueous solution, the mixture was divided equally into 4 parts in glass beakers, then illuminated by the UV irradiation for exposure time intervals of 0, 10, 30, and 45 min. The UV radiation was generated from a Xenon lamp (ORIEL-66005), operating at an output power of $\sim$ 180 W, and the standard emitted wavelength ranges from the UV through visible to near IR spectral region ($\sim$200 nm–900 nm). The distance between the lamp aperture and the solution

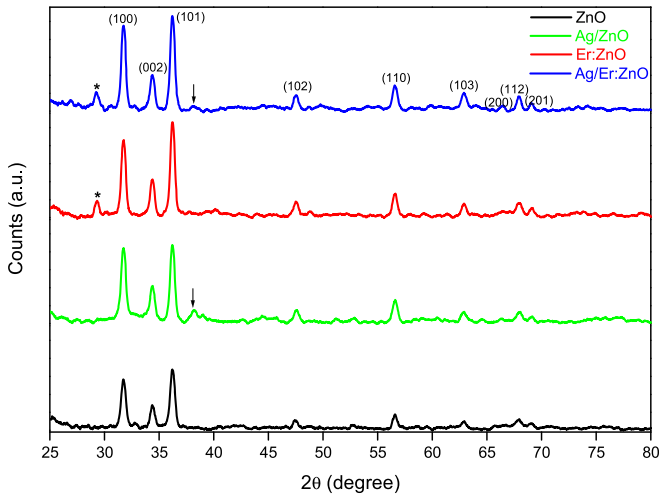

Figure 1. The XRD patterns of ZnO, Er:ZnO, Ag/ZnO, and Ag/Er:ZnO colloidal nanoparticles synthesized via PLAL using bulk targets in double distilled water.

surface was kept at 15 cm. In all samples, the molar concentration of the R6G dye was kept at 10^{-5} M. Before and after UV irradiation, the optical absorption spectra of the R6G dye solutions were recorded by a PG (T80 UV/VIS) spectrophotometer in the visible spectral range. All photocatalytic experiments and measurements were carried out at room temperature.

3. Results and discussions

The XRD patterns of the laser-ablated nanoparticles are represented in figure 1. The observed peaks at around 31.8°, 34.4°, 36.2°, 47.4°, 56.6°, 62.9°, 66.4°, 67.9°, and 69.1° match well with the (100), (002), (101), (102), (110), (103), (200), (112), and (201) planes, respectively, of the indexed hexagonal ZnO crystal structure (COD 2107059). No Zn peaks were observed, probably because the ZnO NPs were ablated directly from stoichiometric bulk targets [16, 61].

The observed peak at around 29.3° (labeled by *) is assigned to the (222) plane of Er_2O_3 dopant [11, 22, 23, 25, 62, 63]. Thus, during the sintering process, at 1 mol % Er_2O_3 doping concentration, some of erbium ions might be aggregated and form a separate phase of Er_2O_3 in the sintered pellet target. In addition, a slight shift of the ZnO diffraction peak (002) toward lower angle was observed in Er:ZnO sample. This could reveal that some of Er^{3+} ions (with ionic radius (0.89 Å) higher than that of Zn^{2+} (0.74 Å)) were partly substituted into the ZnO lattice [21, 25, 64] during the sintering process, and/or the laser ablation. Furthermore, the XRD peak intensity is slightly increased in Er-doped ZnO NPs. This is likely because the laser ablation or fragmentation of undoped ZnO sintered bulk target is harder than that of the doped one [16, 65].

The weak XRD peak at around 38.24° (labeled by ↓) in the hybrid Ag/ZnO and Ag/Er:ZnO samples, is corresponded to the face-centered cubic crystal plane (111) of metallic Ag (COD 1100136) [15, 26, 33–35, 37, 66], and its low intensity may reveal the poor crystallinity and/or the low productivity of the ablated Ag NPs in the present study.

The collected data from the XRD peak, corresponds to the crystal plane (101) of ZnO lattice, was applied to the Debye–Scherrer's formula [67] for estimating the average grain size of the ablated nanoparticles (table 1). For the ZnO and Er:ZnO samples, the estimated average grain size is 19.4 nm and 20.6 nm, respectively.

The constituent elements of the hybrid Ag/Er:ZnO nanoparticles were further identified by the EDXS measurements (figure S1 in the Supplementary Material). And, the estimated mass percentages of the elements Zn, O, Ag, and Er are 57.86, 40.22, 1.23 and 0.68 atomic mass %, respectively, in the scanned area of the sample.

Figures 2(a)–(d) show the TEM images of the laser-ablated ZnO, Er:ZnO, Ag/ZnO, and Ag/Er:ZnO nanoparticles. Most of the ablated NPs have irregular and nearly round shapes and a broad size-distribution with size ranges from ~10 nm to 50 nm.

The nanoparticles were ablated from the bulk targets in distilled water without surfactant, and this could cause the aggregation of the obtained NPs [48, 68]. Moreover, the successive laser pulses in a certain target area could result in continual fragmentation and formation of NPs, beside the random coalescence of the obtained NPs in the aqueous medium [69]. Similar aggregation and broad size-distribution of ZnO NPs synthesized by PLAL were observed in reported studies [16, 48, 55, 69, 70].

Table 1. The XRD analysis and the bandgap energy E_g of the laser-ablated nanoparticles.

Sample	Plane (002)	Plane (101)			E_g (eV)
	2θ (deg)	2θ (deg)	FWHM (deg)	Average grain size (nm)	
ZnO	34.396	36.221	0.43352	19.3	3.13
Er:ZnO	34.372	36.225	0.40686	20.5	3.21
Ag/ZnO	34.369	36.213	0.43023	19.4	3.11
Ag Er:ZnO	34.376	36.222	0.42425	19.7	3.21

In figures 2(c)–(d), the dark spheres are likely metallic silver nanoparticles. In general, the Ag NPs could be distinguished from the ZnO NPs due to their contrast under the transmission electron microscope. The Ag metal has higher electron density than ZnO metal oxide and hence would look darker compared to the ZnO NPs [55]. Furthermore, the metallic nanoparticles, ablated from a bulk metal in liquid medium, commonly have a spherical shape [42, 66].

The crystallinity of the ablated NPs is further revealed by the selected area electron diffraction (SAED) patterns. Moreover, from the HR-TEM images in figures 2(aIII), (bIII), and (dIII), the estimated lattice spacing is 0.18, 0.21, and 0.12 nm and could be assigned to the planes (102), (101), and (201) of the hexagonal ZnO lattice structure, respectively (COD 2107059). In addition, the lattice spacing shown in figure 2(cIII) is 0.15 nm and assigned to the plane (220) of the cubic Ag crystal structure (COD 1100136).

The UV-visible optical absorption spectra of the laser-ablated ZnO, Er:ZnO, Ag/ZnO and Ag/Er:ZnO NPs colloidal samples, are shown in figure 3. In all spectra, the UV absorption peak is attributed to the characteristic interband transition of ZnO semiconductor [55, 66, 68, 71]. In addition, a broad shoulder centered at 412 nm was observed in the spectra of Ag/ZnO and Ag/Er:ZnO NPs hybrid samples, and ascribed to the surface plasmon resonance (SPR) of Ag metallic nanoparticles [55, 66, 67]. The UV absorbance peak intensity is obviously higher in Er:ZnO and Ag/Er:ZnO samples, implying that the ablation yield and NPs productivity of the doped ZnO sintered bulk target are higher than those of the undoped ZnO one [16, 65]. No absorption peaks related to Er_2O_3 ions were resolved in Er-doped ZnO samples.

ZnO is a direct bandgap semiconductor, and the bandgap energy E_g of all samples was estimated using the Tauc plot of $(Ah\nu)^2$ versus $h\nu$ (figure 4), where A is the absorbance intensity in arbitrary unit, and $h\nu$ is the photon energy in eV [58, 72]. For ZnO and Er:ZnO colloidal NPs, E_g was ~ 3.13 and 3.21 eV, respectively, and for the hybrid Ag/ZnO and Ag/Er:ZnO samples, E_g was ~ 3.11 and 3.21 eV, respectively (table 1). Thus, the apparent E_g of Er:ZnO sample is slightly widened compared to that of ZnO NPs, and the observed bandgap widening could be attributed to the Burstein–Moss effect caused by Er-dopants [58, 73]. No obvious change was observed in the ZnO bandgap upon hybridizing ZnO and Er:ZnO NPs colloidal samples with Ag NPs.

The room-temperature Photoluminescence spectra of ZnO, Er:ZnO, Ag/ZnO and Ag/Er:ZnO colloidal NPs are shown in figure 5. The observed near UV emission peak (equivalent to ~ 3.25 eV) is attributed to the characteristic near band-edge exciton emission (NBE) of ZnO semiconductor [34, 55, 68, 72, 74–77]. In addition, broad and weak intensity visible emission bands can be noted and is ascribed to the luminescent defect-states within the ZnO bandgap [34, 55, 68, 75]. No PL emission from erbium (Er^{3+}) ions can be resolved, even under direct excitation (at 488 nm). Thus, in the laser-ablated Er-doped ZnO nanoparticles in water, the characteristics intra-4f radiative transitions of Er^{3+} ions are inactive.

In figures 5(a)–(b), the intensity of the ZnO exciton emission peak decreases in the hybrid Ag/ZnO and Ag/Er:ZnO colloidal NPs, compared to ZnO and Er:ZnO samples, respectively. The quenching of the ZnO exciton emission, when hybridization with noble metal such as Ag NPs, has been observed in previous studies and attributed to the effective separation of the photo-generated electron–hole pairs, at the Ag /ZnO interface [26, 27, 34, 37, 55]. Schottky barrier can be formed at the metal/semiconductor interface, and Ag metal can trap the excited electrons in the ZnO conduction band, and hence reducing the rate of radiative recombination of the photoexcited charge carriers [26, 33, 37, 55].

The photocatalytic response of the laser-ablated ZnO, Er:ZnO, Ag/ZnO, and Ag/Er:ZnO colloidal nanoparticles was examined through the photodegradation of the R6G organic dye. The absorbance spectra of the dye solution containing the colloidal NPs, after different time intervals (0, 10, 30, and 45 min) of UV illumination, are represented in figures 6(b)–(e). For comparison, the absorbance spectra of the blank dye solution after UV illumination for the same time intervals, are shown in figure 6(a). It is obvious that, upon mixing with the laser-ablated NPs, the optical absorption peak intensity of the dye molecules (at ~ 526 nm) decreases as the time interval of UV illumination increases, indicating the photocatalytic decomposition of the organic dye molecules.

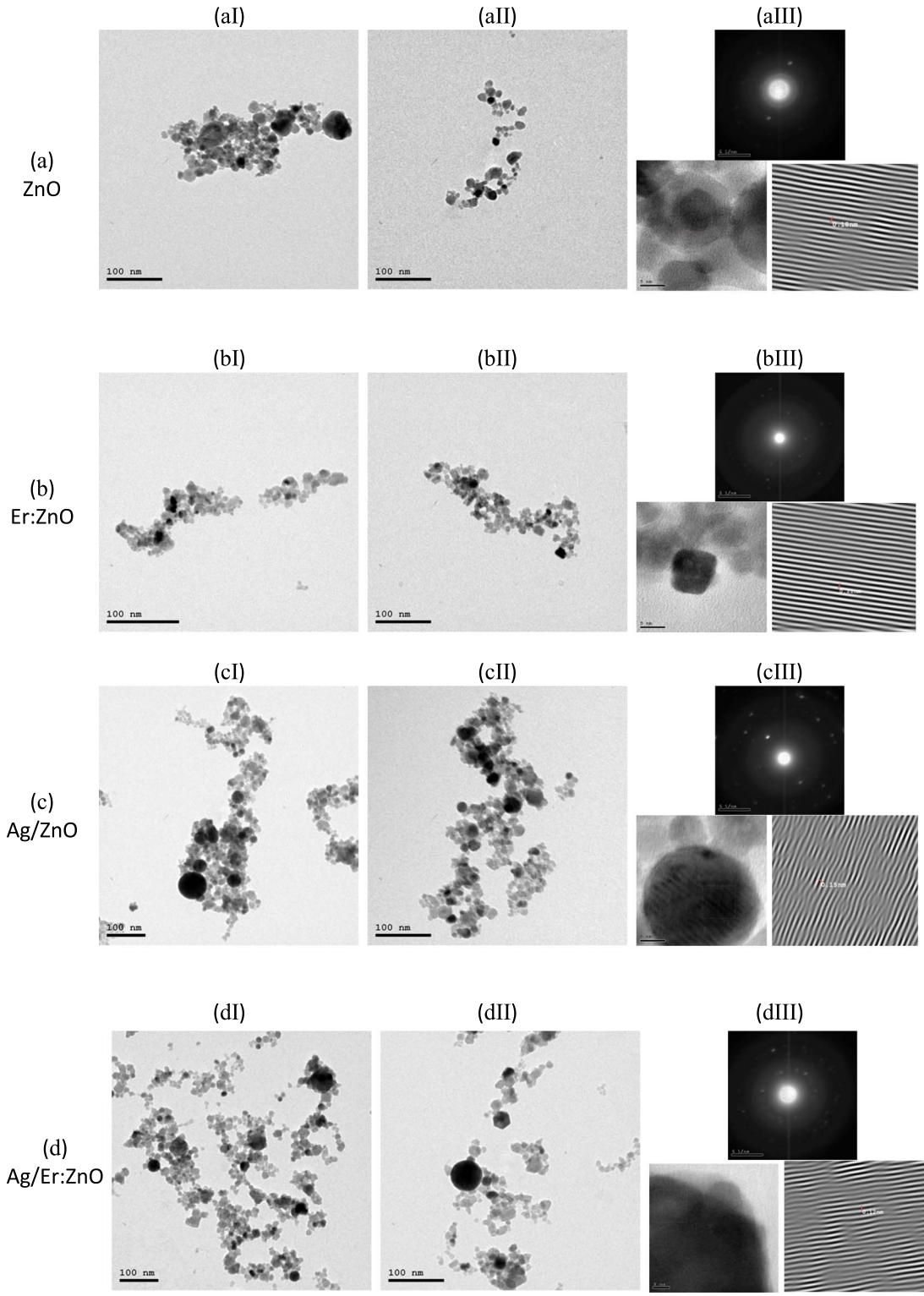

Figure 2. The TEM & HR-TEM images, and SAED patterns of (a) ZnO, (b) Er:ZnO, (c) Ag/ZnO, and (c) AgEr:/ZnO NPs, produced via PLAL using stoichiometric bulk targets in water.

In general, the peak absorbance (A) of the organic dye molecules is directly proportional to the dye concentration (C). Hence, the photodegradation efficiency of the R6G dye molecules can be estimated by [16, 34]:

$$\eta\ (\%) = \left(\frac{A_o\ -\ A_t}{A_o}\right) \times\ 100 = \left(\frac{C_o\ -\ C_t}{C_o}\right) \times\ 100$$

where A_o and C_o are the absorbance and the corresponding concentration, respectively, of the dye molecules before the irradiation, while A_t and C_t are those after illumination with UV light for time interval t. The

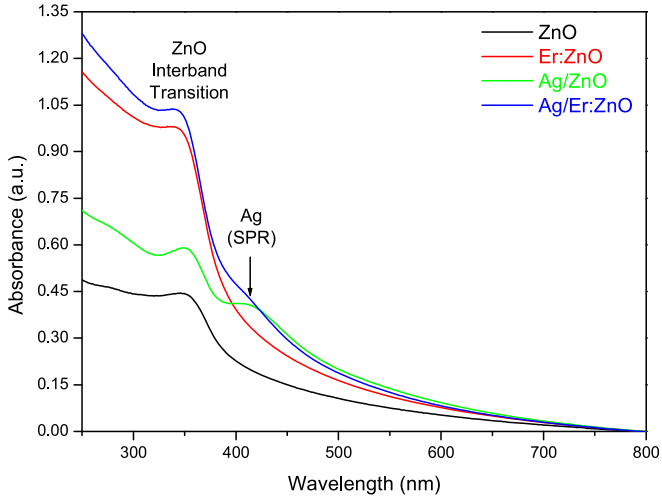

Figure 3. The UV-visible absorbance spectra of the laser-ablated ZnO, Er:ZnO, Ag/ZnO, and Ag/Er:ZnO colloidal nanoparticles.

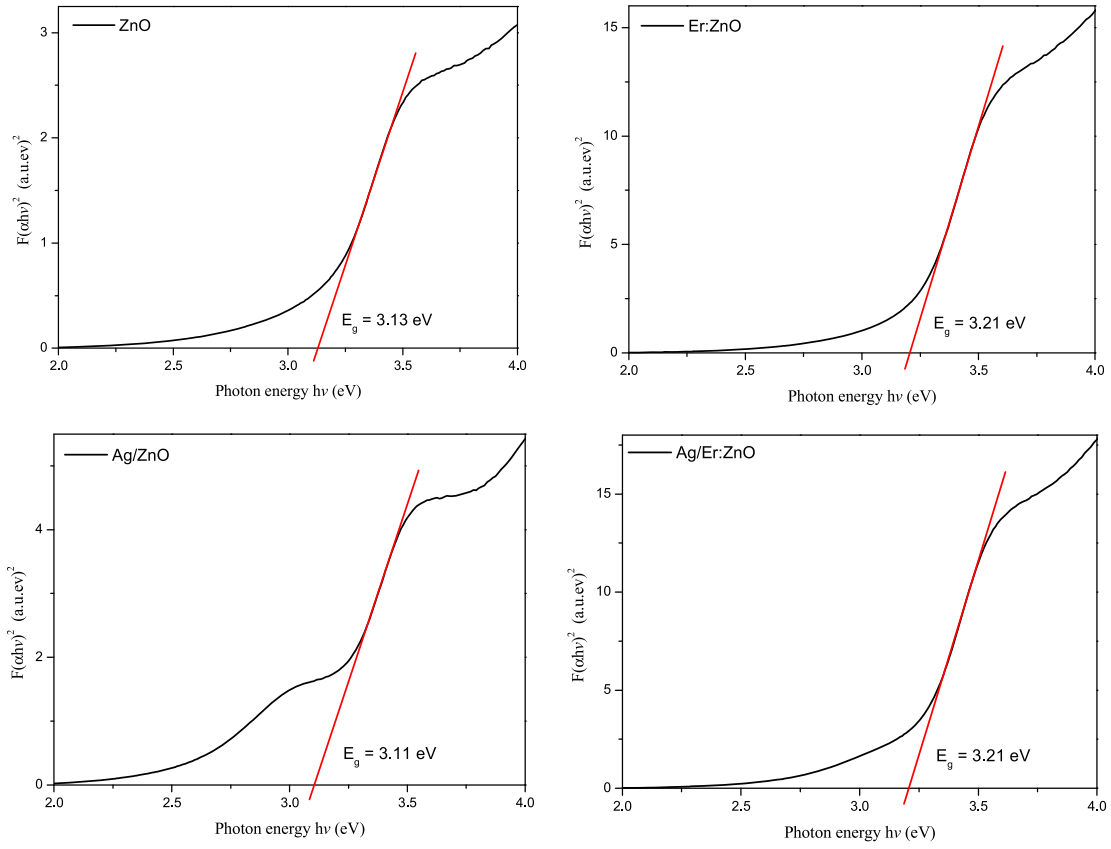

Figure 4. The Tauc plot of $(Ah\upsilon)^2$ versus $(h\upsilon)$ for ZnO, Er:ZnO, Ag/ZnO and Ag/Er:ZnO colloidal NPs.

estimated photodegradation efficiency η (%) is listed in table 2, and plotted versus the irradiation time interval t in figure 7(a).

Scheme 1 depicts the irreversible photocatalytic process, under illumination by UV light, as follows. When ZnO nanoparticles absorb the incident UV photons energy, some electrons in the valance band (VB) are excited to the conduction band (CB) and left behind holes in the valence band. Then, the radical ($^{\bullet}O_2^-$) could be formed by the interaction between the electrons in the CB and the oxygen molecules dissolved in the solution. In addition, the radical ($^{\bullet}OH$) could be produced by the interaction between the holes in the VB and the H_2O molecules, and/or the adsorbed hydroxy (−OH) functional group. Finally, the adsorbed molecules of the

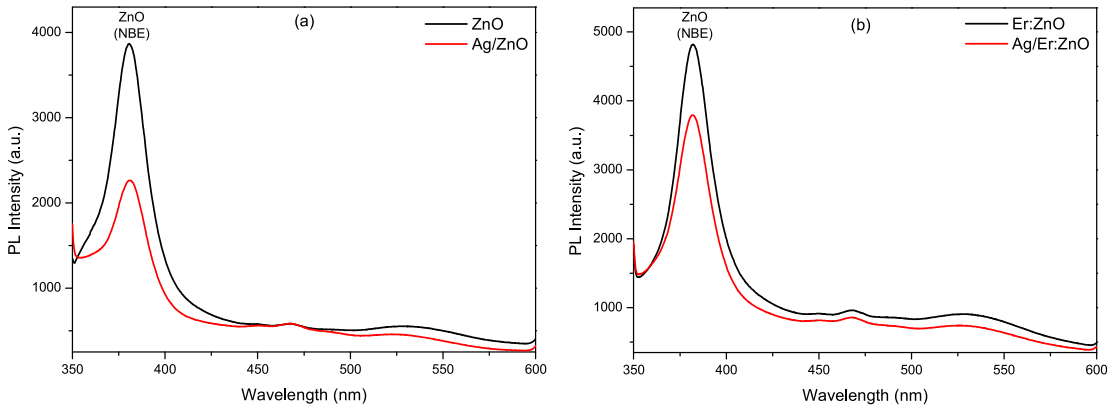

Figure 5. The PL spectra of (a) ZnO, Ag/ZnO, (b) Er:ZnO, and Ag/Er:ZnO colloidal nanoparticles (recorded at room-temperature under excitation wavelength of 325 nm).

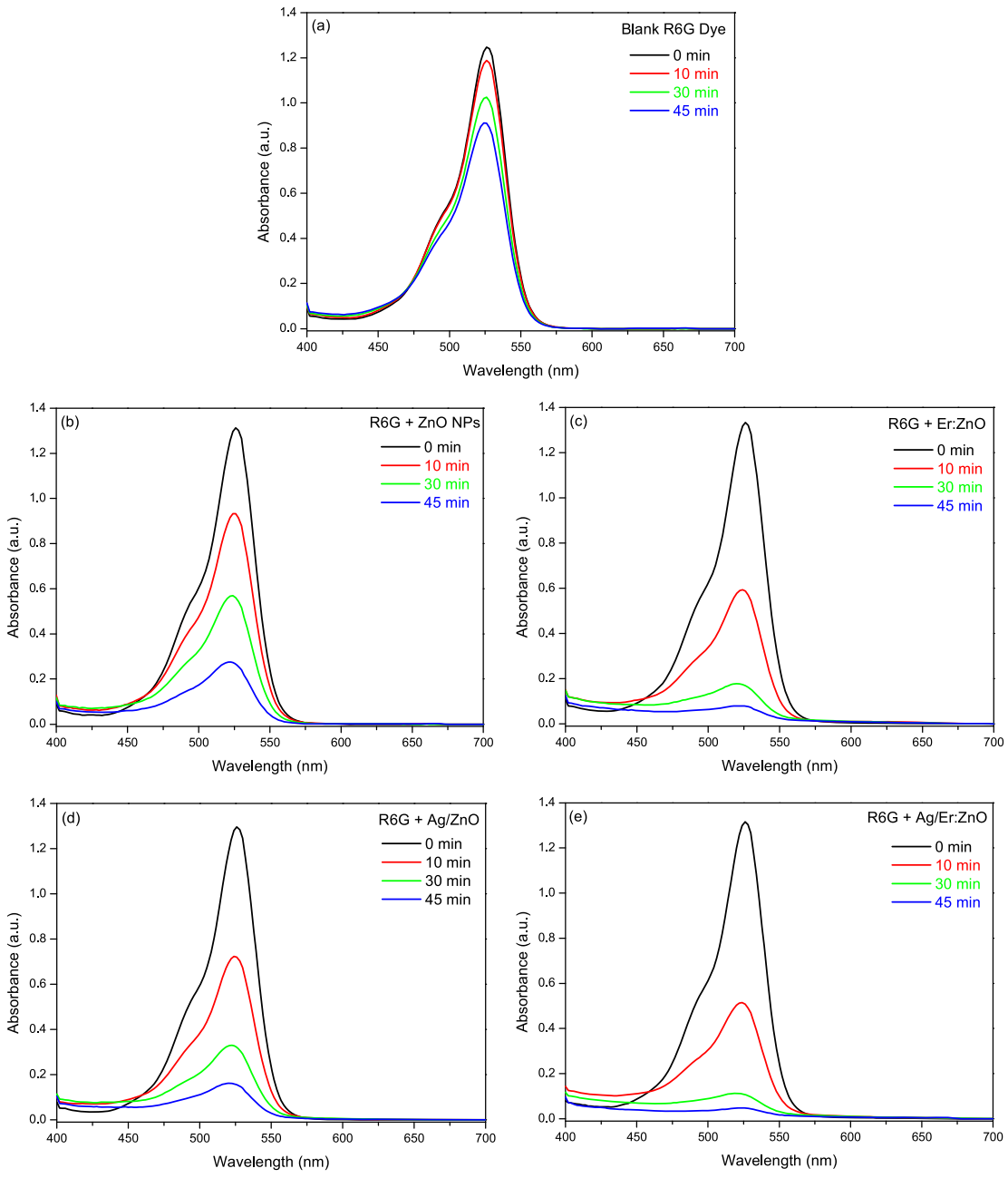

Figure 6. The optical absorbance spectra of (a) the blank R6G dye solution, and (b-e) the R6G dye solution mixed with ZnO, Er:ZnO, Ag/ZnO and Ag/Er:ZnO colloidal NPs, respectively, after different time interval of UV illumination.

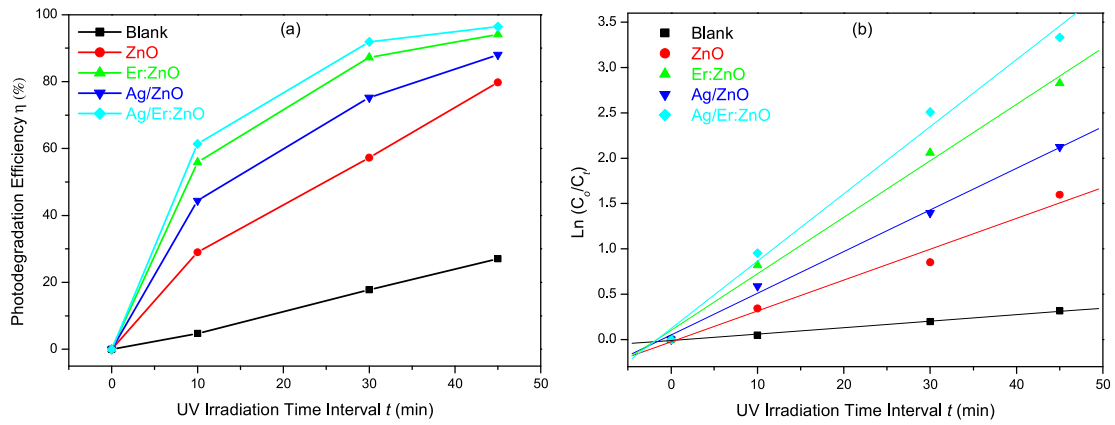

Figure 7. (a) The plots of the photodegradation efficiency η (%) versus the UV illumination time t. (b) The plot of Ln (C_o/C_t) versus t.

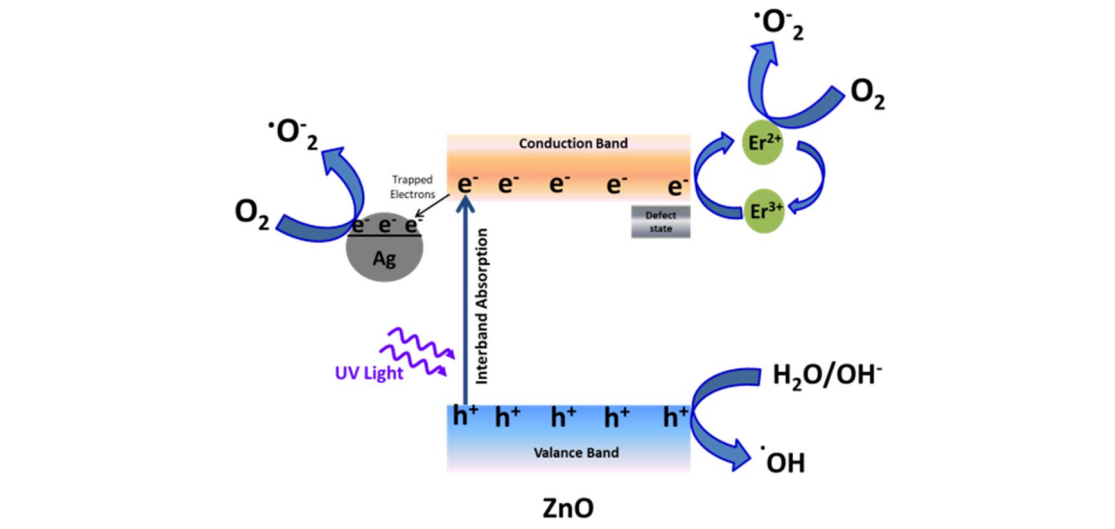

Scheme 1. The photocatalytic mechanism under illumination by UV light, in dye solution containing Ag/Er:ZnO NPs.

Table 2. The photodegradation efficiency η (%) and the rate constant k, for the blank and dye solutions mixed with the NPs.

Sample	The photodegradation efficiency η (%)			The rate constant k (min^{-1})
	10 min	30 min	45 min	
Blank R6G	4.7	17.8	27.0	0.007
ZnO	29.0	57.3	79.7	0.034
Er:ZnO	55.9	87.2	94.1	0.062
Ag/ZnO	44.4	75.2	88.0	0.046
Ag/Er:ZnO	61.4	91.9	96.4	0.074

organic dye pollutant can be degraded by the active superoxide ($^{\cdot}O_2^-$) and hydroxyl ($^{\cdot}OH$) radicals, into inorganic end product [1, 2, 8, 48, 78].

In the blank dye solution (figure 6(a)), the photolysis of the organic R6G molecules dissolved in the distilled water is observed [79], and the estimated degradation efficiency, after 45 min of UV illumination, is 27%. However, in the dye solution containing the ZnO, Ag/ZnO, Er:ZnO, and Ag/Er:ZnO colloidal NPs, the degradation efficiency obviously enhanced to be 79.7, 88, 94.1, and 96.4%, respectively, indicating the photocatalytic nature of the laser-ablated colloidal nanoparticles. The plot of Ln (C_o/C_t) versus the UV

Table 3. Data of the preparation techniques and photocatalytic performance of different ZnO-based photocatalysts, collected from reported studies in the literature.

Nanomaterial	Preparation technique	Photocatalysis reaction time/photon source	Photo-degradation efficiency	Organic pollutant/concentration	References
Ag/Er:ZnO	PLAL	45 min/UV illumination	96.4%	Rhodamine 6G (R6G) dye/10^{-5} M	The present study
Au/Eu:ZnO	PLAL	45 min/UV illumination	92.8%	R6G dye/10^{-5} M	[16]
0.8 at% Ag-ZnO	PLAL	120 min/UV (A-B) light	90%	R6G dye/5 μM	[55]
0.32 wt% Ag- ZnO	PLAL	60 min/UV illumination	73%	Methylene Blue (MB) dye /2.7 $\times$ 10^{-5} mol/L	[36]
1.62 wt% Eu:ZnO	Forced-Hydrolysis Method	80 min/UV–visible light	99.3%	MB dye/0.0267 mM	[17]
1 mol% Eu:ZnO	Chemical Precipitation Method	180 min/UV light	95.3%	Methyl Orange (MO) dye/10 mg L^{-1}	[18]
Er^{3+}:$YAlO_3$/ZnO composite	Ultrasonic Dispersion & Liquids Boiling Method	60 min/solar light	86.4%	Acid Red B dye/10 mg L^{-1}	[20]
2.5 wt% Er-ZnO	Combustion Method	60 min/UV irradiation	99.1%	Direct Red 31 (DR-31) dye	[22]
0.6 wt% Er^{3+}-ZnO	Solid-State Reaction Technique	25 min/UV light	96.7%	MB dye/10^{-5} M	[23]
0.09 mmol Er-ZnO	Sol–Gel Method	60 min/UV–visible light	90%	Phenol/20 mg L^{-1}	[24]
Ag/ZnO/PMMA	Low-Temperature Atomic Layer Deposition (ALD) on Poly (Methyl Methacrylate) (PMMA)	4 h/UV light	90%	Sodium Lauryl Sulfate (SDS)/1.5 $\times$ 10^{-5} M	[26]
1.7% Ag -ZnO	Hydrothermal Technique Followed By Pulsed Laser Depositing of Ag	120 min/UV (A-B) light	86%	R6G dye	[27]
Ag/ZnO	Hydrothermal Method	40 min/Sunlight illumination	96.7%	Rhodamine B (RhB) dye	[32]
Ag-ZnO core–shell	Atomic Layer Deposition (ALD) on Ag Cores	100 min/Artificial Sunlight	98%	RhB dye/10^{-5} M	[39]
0.5 at.% Ag- ZnO	Microwave-Assisted Technique	5 h/Solar light irradiation	98.5%	Phenol	[33]
3 mol% Ag -ZnO	Modified Polymer-Network Gel Method	25 min/Simulated Sunlight	100%	MB/4 mg L^{-1}	[34]
1 wt% Ag-deposited ZnO	Photodeposition Method	60 min/UV irradiation	99%	Levofloxacin/1 g L^{-1}	[35]
3 wt% Ag-ZnO	Combined Sol–Gel & Chemical Reduction Method	240 min/UV irradiation visible light	82.6% 76%	MB dye/2$\times$$10^{-5}$M	[37]

illumination time interval t (figure 7(b)) shows that the photocatalytic degradation process exhibits a pseudo first-order kinetics, with a rate constant k, as follows [25, 55]:

$$Ln\left(\frac{C_o}{C_t}\right) = kt$$

The rate constant k (estimated from the linear fitting of the plot) is 0.007 min^{-1} in the blank dye solution, while in dye solution containing the ZnO, Ag/ZnO, Er:ZnO, and Ag/Er:ZnO colloidal NPs, k is 0.034, 0.046, 0.062, and 0.074 min^{-1}, respectively. The hybrid Ag/Er:ZnO colloidal NPs presented the highest photocatalytic response.

Doping ZnO lattice with 1 mol % of Er_2O_3 could introduce some point defects and trapping sites, which can enhance the separation of the photo-generated charges, and consequently, the photocatalytic activity of the ZnO NPs. And the higher concentration of the ablated NPs in colloidal sample ablated from Er:ZnO bulk, as revealed by the absorbance spectra, could also attributed to the enhanced photocatalytic response of Er:ZnO NPs colloidal sample [16, 23]. Moreover, the trivalent erbium ions (Er^{3+}) dopants may capture electrons from ZnO conduction band and be reduced to Er^{2+} ions, which consequently could form the active radical ($^{\bullet}O_2^-$) via the interaction with the dissolved oxygen molecules [13, 24, 25].

In addition, the Ag NPs could act as electrons traps at the metal/semiconductor (Ag/ZnO) Schottky barrier interface, reducing the charges-recombination rate [26, 27, 33, 37, 55], as revealed by the PL spectra, and enhancing of the photocatalytic response of ZnO NPs in hybrid Ag/ZnO and Ag/Er:ZnO NPs colloidal samples. Thus, the accumulated effects of the Er-doping and adding Ag NPs obviously enhance the photocatalytic performance of ZnO nanoparticles in the hybrid Ag/Er:ZnO colloidal NPs sample. Furthermore, the listed data in table 2 show that the effect of Er_2O_3 doping on the photocatalytic efficiency of ZnO NPs is higher than that of adding Ag NPs, in the present study.

The direct comparison between the obtained results and those of previous works is somehow difficult because of the differences in the preparation techniques and the photocatalytic experimental parameters. However, for rough comparison, the data of the photocatalytic performance of different ZnO-based photocatalysts, collected from reported studies in the literature and the present study, are listed in table 3. For instance, 90% of R6G dye was degraded during 120 min of UV illumination in the presence of ZnO–Ag nanoparticles, synthesized via PLAL using Zn and Ag plates in aquabides [55], while in current study about 96% of the R6G dye was degraded in 45 min of UV illumination.

Furthermore, the obtained results of the current work, when compared with those of our previous study [16], show that the laser-ablated Ag/Er:ZnO colloidal NPs possess enhanced photocatalytic activity similar to those of the Au/Eu:ZnO. These findings in turns emphasize that the pulsed laser ablation of bulk targets in pure water is a reliable, fast, and echo-friendly technique for producing hybrid noble metal/rare-Earth doped semiconductor colloidal nanoparticles with photocatalytic nature. Moreover, the photocatalytic performance of ZnO semiconducting nanoparticles was significantly enhanced upon doping with the trivalent rare-Earth oxides (Eu^{3+} or Er^{3+}) and mixing with the noble metals (Au or Ag).

4. Conclusion

In the present study, ZnO, Er:ZnO, Ag/ZnO, and Ag/Er:ZnO colloidal NPs catalysts were produced via PLAL using bulk targets in double distilled water without any surfactant. The polycrystalline nature of the laser-ablated NPs has been confirmed by the XRD analysis. The TEM images showed aggregated nanoparticles with irregular round shapes and the size ranges from about 10 nm to 50 nm. The photocatalytic response of the laser-ablated nanoparticles was examined by the degredation of the organic R6G dye, under UV illumination. The degradation efficiency, after 45 min of UV illumination, was estimated to be 79.7, 88, 94.1, and 96.4%, of the dye solution containing the ZnO, Ag/ZnO, Er:ZnO, and Ag/Er:ZnO NPs, respectively. These results confirm the enhancement of the photocatalytic performance of ZnO upon hybridization with the selected dopants, and indicate that efficient hybrid nanomaterials for photocatalysis applications can be produced by the simple and reliable PLAL technique.

In the future work, we plan to immobilize the laser-ablated Ag/Er:ZnO and/or Au/Eu:ZnO nanoparticles in appropriate polymer and investigate their photocatalytic performance.

Acknowledgments

We thank Professor Gamal Abdel Fattah from the National Institute of Laser Enhanced Sciences, Cairo University, for his help in the photocatalysis measurements.

Data availability statement

All data that support the findings of this study are included within the article (and any supplementary files).

Supplementary data

Figure of the EDXS data of the hybrid Ag/Er:ZnO NPs.

ORCID iDs

Samah M Ahmed https://orcid.org/0000-0002-6588-2599

References

[1] Rajput R B, Shaikh R, Sawant J and Kale R B 2022 Recent developments in ZnO-based heterostructures as photoelectrocatalysts for wastewater treatment: a review *Environmental Advances* **9** 100264
[2] Sanakousar F M, Vidyasagar C C, Jiménez-Pérez V M and Prakash K 2022 Recent progress on visible-light-driven metal and non-metal doped ZnO nanostructures for photocatalytic degradation of organic pollutants *Mater. Sci. Semicond. Process.* **140** 106390
[3] Al Ja'farawy M S, Kusumandari K, Purwanto A and Widiyandari H 2022 Carbon quantum dots supported zinc oxide (ZnO/CQDs) efficient photocatalyst for organic pollutant degradation—a systematic review *Environmental Nanotechnology, Monitoring & Management* **18** 100681
[4] Waghchaure R H, Adole V A and Jagdale B S 2022 Photocatalytic degradation of methylene blue, rhodamine B, methyl orange and eriochrome black T dyes by modified ZnO nanocatalysts: a concise review *Inorg. Chem. Commun.* **143** 109764
[5] Gao W, Liu Y and Dong J 2021 Immobilized ZnO based nanostructures and their environmental applications *Progress in Natural Science: Materials International* **31** 821–34
[6] Ong C B, Ng L Y and Mohammad A W 2018 A review of ZnO nanoparticles as solar photocatalysts: synthesis, mechanisms and applications *Renewable and Sustainable Energy Reviews 81, Part* **1** 536–51
[7] Goktas S and Goktas A 2021 A comparative study on recent progress in efficient ZnO based nanocomposite and heterojunction photocatalysts: a review *J. Alloys Compd.* **863** 158734
[8] Ahmad I, Shukrullah S, Naz M Y, Bhatti H N, Ahmad M, Ahmed E, Ullah S and Hussien M 2022 Recent progress in rare earth oxides and carbonaceous materials modified ZnO heterogeneous photocatalysts for environmental and energy applications *J. Environ. Chem. Eng.* **10** 107762
[9] Munawar T, Yasmeen S, Mukhtar F, Nadeem M S, Mahmood K, Saqib Saif M, Hasan M, Ali A, Hussain F and Iqbal F 2020 $Zn_{0.9}Ce_{0.05}M_{0.05}O$ (M = Er, Y, V) nanocrystals: Structural and energy bandgap engineering of ZnO for enhancing photocatalytic and antibacterial activity *Ceram. Int.* **46** Part A 14369–83
[10] Pascariu P, Cojocaru C, Olaru N, Samoila P, Airinei A, Ignat M, Sacarescu L and Timpu D 2019 Novel rare earth (RE-La, Er, Sm) metal doped ZnO photocatalysts for degradation of congo-red dye: synthesis, characterization and kinetic studies *J. Environ. Manage.* **239** 225–34
[11] Zhao S, Shen Y, Li A, Chen Y, Gao S, Liu W and Wei D 2021 Effects of rare Earth elements doping on gas sensing properties of ZnO nanowires *Ceram. Int.* **47** 24218–26
[12] Kumar S G and Kavitha R 2021 Lanthanide ions doped ZnO based photocatalysts *Sep. Purif. Technol.* **274** 118853
[13] Pandiyarajan T, Mangalaraja R V, Karthikeyan B, Udayabhaskar R, Contreras D, Sepulveda-Guzman S and Gracia-Pinilla M A 2022 Influence of RE (Pr^{3+}, Er^{3+}, Nd^{3+}) doping on structural, vibrational and enhanced persistent photocatalytic properties of ZnO nanostructures *Spectrochimica Acta Part A: Molecular and Biomolecular Spectroscopy* **268** 120679
[14] Palanivel B, Macadangdang Jr R R, Hossain M S, Alharthi F A, Kumar M, Chang J-H and Gedi S 2023 Rare earth (Gd, La) co-doped ZnO nanoflowers for direct Sunlight driven photocatalytic activity *J. Rare Earths* **41** 77–84
[15] Lee M, Lee H-S, Kim M Y, Lee K H and Lee W 2022 Significant improvement in the acetone sensing performance of Ag-decorated ZnO porous nanosheets through defect engineering by Li-ion implantation *Sensors Actuators* B **372** 132671
[16] Ahmed S M and Imam H 2020 Characterization and photocatalytic activity of Eu:ZnO & Au/Eu:ZnO nanoparticles prepared by laser ablation in water *Mater. Sci. Semicond. Process.* **115** 105128
[17] H-Carrilloa M A, T-Ricárdeza R, G-Mendozaa M F, R-Moralesa E, R-Blancoa L, D-Floresa L L, S-Palaciosb G E, P-Delgadoc F and P-Hernándeza G 2020 Eu-modified ZnO nanoparticles for applications in photocatalysis *Catal. Today* **349** 191–7
[18] Zong Y, Li Z, Wang X, Ma J and Men Y 2014 Synthesis and high photocatalytic activity of Eu-doped ZnO nanoparticles *Ceram. Int.* **40** 10375–82
[19] Gong X *et al* 2022 Achieving efficient photocatalytic uranium extraction within a record short period of 3 min by Up-conversion erbium doped ZnO nanosheets *Chem. Eng. J.* **450** 138044
[20] Wang J, Xie Y, Zhang Z, Li J, Chen X, Zhang L, Xu R and Zhang X 2009 Photocatalytic degradation of organic dyes with Er^{3+}:$YAlO_3$/ZnO composite under solar light *Solar Energy Materials & Solar Cells* **93** 355–61
[21] Sin J-C, Lam S-M, Lee K-T and Mohamed A R 2013 Fabrication of erbium-doped spherical-like ZnO hierarchical nanostructures with enhanced visible light-driven photocatalytic activity *Mater. Lett.* **91** 1–4
[22] Bhatia S, Verma N and Bedi R K 2016 Optical application of Er-doped ZnO nanoparticles for photodegradation of direct red − 31 dye *Opt. Mater.* **62** 392–8
[23] Divya N K and Pradyumnan P P 2016 Solid state synthesis of erbium doped ZnO with excellent photocatalytic activity and enhanced visible light emission *Mater. Sci. Semicond. Process.* **41** 428–35
[24] Sowik J, Miodyńska M, Bajorowicz B, Mikolajczyk A, Lisowski W, Klimczuk T, Kaczor D, Medynska A Z and Malankowska A 2019 Optical and photocatalytic properties of rare Earth metal-modified ZnO quantum dots *Appl. Surf. Sci.* **464** 651–63
[25] AlAbdulaal T, AlShadidi M, Hussien M, Ganesh V, Bouzidi A, Rafique S, Algarni H, Zahran H, Abdel-wahab M and Yahia I 2022 Multifunctional and smart Er_2O_3–ZnO nanocomposites for electronic ceramic varistors and visible light degradation of wastewater treatment *Environmental Science and Pollution Research* **29** 19109–31

[26] Mauro A D *et al* 2020 Ag/ZnO/PMMA Nanocomposites for Efficient Water Reuse *ACS Appl. Bio Mater.* **3** 4417–26
[27] Yudasari N, Dinata K H, Shearer C J, Blanco-Sanchez P H, Tresna W P, Isnaeni, Suliyanti M M and Trilaksana H 2022 Laser-assisted deposition of Ag on self-sourced growth ZnO nanorods as reusable photocatalysts for water purification *Inorg. Chem. Commun.* **146** 110065
[28] Ali H, Ismail A M and Menazea A A 2022 Multifunctional Ag/ZnO/chitosan ternary bio-nanocomposites synthesized via laser ablation with enhanced optical, antibacterial, and catalytic characteristics *Journal of Water Process Engineering* **49** 102940
[29] Farooq M, Shujah S, Tahir K, Nazir S, Khan A U, Almarhoon Z M, Jevtovic V, Al-Shehri H S, Hussain S T and Ullah A 2022 Ultra efficient 4-Nitrophenol reduction, dye degradation and Cr(VI) adsorption in the presence of phytochemical synthesized Ag/ZnO nanocomposite: a view towards sustainable chemistry *Inorg. Chem. Commun.* **136** 109189
[30] Ifijen I H, Maliki M and Anegbe B 2022 Synthesis, photocatalytic degradation and antibacterial properties of selenium or silver doped zinc oxide nanoparticles: A detailed review *Open Nano* **8** 100082
[31] Zhang Q, Li J and Xu M 2022 Ag-decorated ZnO-based nanocomposites for visible light-driven photocatalytic degradation: basic understanding and outlook *J. Phys. D* **55** 483001
[32] Guo Y, Fu X, Xie Y, Zhu L, Liu R and Liu L 2022 Synthesis of Ag/ZnO nanocomposites with enhanced visible photocatalytic performance *Opt. Mater.* **133** 112980
[33] Al Ghafry S S A, Al Shidhani H, Al Farsi B, Sofin R G S, Al-Hosni A S, Alsharji Z, Al-Sabahi J and Al-Abri M Z 2023 The photocatalytic degradation of phenol under solar irradiation using microwave-assisted Ag-doped ZnO nanostructures *Opt. Mater.* **135** 113272
[34] Liu Y, Zhang Q, Xu M, Yuan H, Chen Y, Zhang J, Luo K, Zhang J and You B 2019 Novel and efficient synthesis of Ag-ZnO nanoparticles for the sunlight-induced photocatalytic degradation *Appl. Surf. Sci.* **476** 632–40
[35] Jandaghian F, Pirbazari A E, Tavakoli O, Asasian-Kolur N and Sharifian S 2023 Comparison of the performance of Ag-deposited ZnO and TiO_2 nanoparticles in levofloxacin degradation under UV/visible radiation *Journal of Hazardous Materials Advances* **9** 100240
[36] Blažeka D, Radičić R, Maletić D, Živković S, Momčilović M and Krstulović N 2022 Enhancement of methylene blue photodegradation rate using laser synthesized Ag-doped ZnO nanoparticles *Nanomaterials* **12** 2677
[37] Abdel Messih M F, Ahmed M A, Soltan A and Anis S S 2019 Synthesis and characterization of novel Ag/ZnO nanoparticles for photocatalytic degradation of methylene blue under UV and solar irradiation *J. Phys. Chem. Solids* **135** 109086
[38] Shaikh A A, Patil M R, Jagdale B S and Adole V A 2023 Synthesis and characterization of Ag doped ZnO nanomaterial as an effective photocatalyst for photocatalytic degradation of Eriochrome Black T dye and antimicrobial agent *Inorg. Chem. Commun.* **151** 110570
[39] Seong S, Park I-S, Jung Y C, Lee T, Kim S Y, Park J S, Ko J-H and Ahn J 2019 Synthesis of Ag-ZnO core–shell nanoparticles with enhanced photocatalytic activity through atomic layer deposition *Mater. Des.* **177** 107831
[40] Danilenko I *et al* 2019 Photocatalytic activity of ZnO nanopowders: the role of production techniques in the formation of structural defects *Catal. Today* **328** 99–104
[41] Uribe-López M C, Hidalgo-López M C, López-González R, Frías-Márquez D M, Núñez-Nogueira G, Hernández-Castillo D and Alvarez-Lemus M A 2021 Photocatalytic activity of ZnO nanoparticles and the role of the synthesis method on their physical and chemical properties *J. Photochem. Photobiol., A* **404** 112866
[42] Zhang D, Gökce B and Barcikowski S 2017 Laser synthesis and processing of colloids: fundamentals and applications *Chem. Rev.* **117** 3990–4103
[43] Alkallas F H, Ahmed H A, Pashameah R A, Alrefaee S H, Toghan A, Trabelsi A B G and Mostaf A M 2022 Nonlinearity enhancement of multi-walled carbon nanotube decorated with ZnO nanoparticles prepared by laser assisted method *Opt. Laser Technol.* **155** 108444
[44] Shankar P, Ishak M Q H, Padarti J K, Mintcheva N, Iwamori S, Gurbatov S O, Lee J H and Kulinich S A 2020 ZnO@graphene oxide core@shell nanoparticles prepared via one-pot approach based on laser ablation in water *Appl. Surf. Sci.* **531** 147365
[45] Naik S S, Lee S J, Begildayeva T, Yu Y, Lee H and Choi M Y 2020 Pulsed laser synthesis of reduced graphene oxide supported ZnO/Au nanostructures in liquid with enhanced solar light photocatalytic activity *Environ. Pollut.* **266** 115247
[46] Lee S J, Begildayeva T, Jung H J, Koutavarapu R, Yu Y, Choi M and Choi M Y 2021 Plasmonic ZnO/Au/g-C3N4 nanocomposites as solar light active photocatalysts for degradation of organic contaminants in wastewater *Chemosphere* **263** 128262
[47] Naik S S, Lee S J, Yeon S, Yu Y and Choi M Y 2021 Pulsed laser-assisted synthesis of metal and nonmetal-codoped ZnO for efficient photocatalytic degradation of Rhodamine B under solar light irradiation *Chemosphere* **274** 129782
[48] Mintcheva N, Aljulaih A A, Wunderlich W, Kulinich S A and Iwamori S 2018 Laser-ablated ZnO nanoparticles and their photocatalytic activity toward organic pollutants *Materials* **11** 1127
[49] Guillén G G, Palma M I M, Krishnan B, Avellaneda D, Castillo G A, Das Roy T K and Shaji S 2015 Structure and morphologies of ZnO nanoparticles synthesized by pulsed laser ablation in liquid: effects of temperature and energy fluence *Mater. Chem. Phys.* **162** 561–70
[50] Camarda P *et al* 2020 Synthesis of multi-color luminescent ZnO nanoparticles by ultra-short pulsed laser ablation *Appl. Surf. Sci.* **506** 144954
[51] Chen W, Yao C, Gan J, Jiang K, Hu Z, Lin J, Xu N, Sun J and Wu J 2020 ZnO colloids and ZnO nanoparticles synthesized by pulsed laser ablation of zinc powders in water *Mater. Sci. Semicond. Process.* **109** 104918
[52] Khudiar S S, Nayef U M and Mutlak F A H 2021 Preparation and characterization of ZnO nanoparticles via laser ablation for sensing NO_2 gas *Optik* **246** 167762
[53] Jawad K H 2023 Laser ablation mediated ZnO nanoparticles inhibit growth and biofilm forming potential of urinary tract bacterium proteus mirabilis *Adv. Nat. Sci.: Nanosci. Nanotechnol.* **14** 015002
[54] Park J, Kim J, Min A and Choi M Y 2022 Fabrication of nonenzymatic electrochemical sensor based on Zn@ZnO core–shell structures obtained via pulsed laser ablation for selective determination of hydroquinone *Environ. Res.* **204** 112340
[55] Yudasari N, Anugrahwidya R, Tahir D, Suliyanti M M, Herbani Y, Imawan C, Khalil M and Djuhana D 2021 Enhanced photocatalytic degradation of rhodamine 6G (R6G) using ZnO–Ag nanoparticles synthesized by pulsed laser ablation in liquid (PLAL) *J. Alloys Compd.* **886** 161291
[56] Elsayed K A, Alomari M, Drmosh Q A, Alheshibri M, Al Baroot A, Kayed T S, Manda A A and Al-Alotaibi A L 2022 Fabrication of ZnO-Ag bimetallic nanoparticles by laser ablation for anticancer activity *Alexandria Engineering Journal* **61** 1449–57
[57] Kanakkillam S S, Krishnan B, Peláez R F C, Martinez J A A, Avellaneda D A and Shaji S 2021 Hybrid nanostructures of Ag/Au-ZnO synthesized by pulsed laser ablation/irradiation in liquid *Surfaces and Interfaces* **27** 101561
[58] Tarasenka N, Kornev V, Ramanenka A, Li R and Tarasenko N 2022 Photoluminescent neodymium-doped ZnO nanocrystals prepared by laser ablation in solution for NIR-II fluorescence bioimaging *Heliyon* **8** 09554
[59] Katsuki D, Sato T, Suzuki R, Nanai Y, Kimura S and Okuno T 2012 *Red luminescence of* Eu^{3+} *doped ZnO nanoparticles fabricated by laser ablation in aqueous solution Appl. Phys.* A **108** 321–7
[60] Ahmed S M, Szymanski P, El-Nadi L M and El-Sayed M A 2014 Energy-transfer efficiency in Eu-doped ZnO thin films: the effects of oxidative annealing on the dynamics and the intermediate defect states *ACS Appl. Mater. Interfaces* **6** 1765–72

[61] Lau M and Barcikowski S 2015 Quantification of mass-specific laser energy input converted into particle properties during picosecond pulsed laser fragmentation of zinc oxide and boron carbide in liquids *Appl. Surf. Sci.* **348** 22–9
[62] Achehboune M, Khenfouch M, Boukhoubza I, Derkaoui I, Leontie L, Carlescu A, Mothudi B M, Zorkani I and Jorio A 2022 Optimization of the luminescence and structural properties of Er-doped ZnO nanostructures: effect of dopant concentration and excitation wavelength *J. Lumin.* **246** 118843
[63] Buryi M, Neykova N, Ridzoňová K, Remeš Z, Děcká K, Hájek F, Artemenko A, Mičová J, Landová L and Jakubec I 2023 Peculiarities of erbium incorporation into ZnO microrods at high doping level leading to upconversion and the morphology change. Influence on excitonic as well as shallow donor states *Appl. Surf. Sci.* **611** 155651
[64] Ahmad I 2019 Inexpensive and quick photocatalytic activity of rare Earth (Er, Yb) co-doped ZnO nanoparticles for degradation of methyl orange dye *Sep. Purif. Technol.* **227** 115726
[65] Krstulović N, Salamon K, Budimlija O, Kovač J, Dasović J, Umek P and Capan I 2018 Parameters optimization for synthesis of Al-doped ZnO nanoparticles by laser ablation in water *Appl. Surf. Sci.* **440** 916–25
[66] D'Urso L, Santangelo S, Spadaro S, Scibilia S, Mezzasalma A M, Neri F and Fazio E 2016 Enhanced optical response of ZnO/Ag nanocolloids prepared by a picosecond laser *J. Lumin.* **178** 204–9
[67] Anugrahwidya R, Yudasari N and Tahir D 2020 Optical and structural investigation of synthesis ZnO/Ag Nanoparticles prepared by laser ablation in liquid *Mater. Sci. Semicond. Process.* **105** 104712
[68] Hu X, Gong H, Xu H, Wei H, Cao B, Liu G, Zeng H and Cai W 2011 Influences of Target and Liquid Media on Morphologies and Optical Properties of ZnO Nanoparticles Prepared by Laser Ablation in Solution *J. Am. Ceram. Soc.* **94** 4305–9
[69] Kim K K, Kim D, Kim S K, Park S M and Song J K 2011 Formation of ZnO nanoparticles by laser ablation in neat water *Chem. Phys. Lett.* **511** 116–20
[70] Camarda P, Schneider R, Popescu R, Vaccaro L, Messina F, Buscarino G, Agnello S, Gelardi F M and Cannas M 2016 Effect of thermal annealing on the luminescence of defective ZnO nanoparticles synthesized by pulsed laser ablation in water *Physica Status Solidi* **13** 1–5 C
[71] Gavrilenko E A, Goncharova D A, Lapin I N, Nemoykina A L, Svetlichnyi V A, Aljulaih A A, Mintcheva N and Kulinich S A 2019 Comparative study of physicochemical and antibacterial properties of ZnO nanoparticles prepared by laser ablation of Zn target in water and air *Materials* **12** 186
[72] Navasa M P, Sonia R K, Tarasenka N and Tarasenko N 2017 Temperature and solution assisted synthesis of anisotropic ZnO nanostructures by pulsed laser ablation *Appl. Surf. Sci.* **414** 413–23
[73] Sánchez-López A L *et al* 2022 Influence of erbium doping on zinc oxide nanoparticles: structural, optical and antimicrobial activity *Appl. Surf. Sci.* **575** 151764
[74] Rezaie M N, Mohammadnejad S and Ahadzadeh S 2021 Hybrid inorganic–organic light-emitting heterostructure devices based on ZnO *Opt. Laser Technol.* **138** 106896
[75] Dasha D, Pandab N R and Sahu D 2019 Photoluminescence and photocatalytic properties of europium doped ZnO nanoparticles *Appl. Surf. Sci.* **494** 666–74
[76] Lee Y, Lee D J, Cho H D, Yoon I T, Shon Y and Lee S 2017 Thermodynamic behaviors of excitonic emission in ZnO nanorods grown by pulsed laser deposition *J. Lumin.* **190** 314–8
[77] Og. Dikovska A, Pallotti D, Lettieri S, Atanasova G B, Avdeev G V, Maddalena P, Amoruso S and Nedyalkov N N 2017 Growth mechanism of ZnO nanostructures produced by ultraviolet and visible laser ablation *Appl. Surf. Sci.* **423** 977–82
[78] Cerrato E, Gionco C, Berruti I, Sordello F, Calza P and Paganini M C 2018 Rare Earth ions doped ZnO: synthesis, characterization and preliminary photoactivity assessment *J. Solid State Chem.* **264** 42–7
[79] Haimerl J M, Ghosh I, König B, Lupton J M and Vogelsang J 2018 Chemical photocatalysis with rhodamine 6G: investigation of photoreduction by simultaneous fluorescence correlation spectroscopy and fluorescence lifetime measurements *J. Phys. Chem.*B **122** 10728–35